

Topological surface states in superconducting CaBi₂

Qi Jiang,^{1,2} Deyang Wang,^{1,2} Zhengtai Liu,^{1,2} Zhicheng Jiang,^{1,2} Haoji Qian,^{1,2} Xiaoping Shen,³ Ang Li,^{1,2} Dawei Shen^{1,2} ,
Shan Qiao,^{1,2,4,*} and Mao Ye^{1,2,†}

¹State Key Laboratory of Functional Materials for Informatics, Shanghai Institute of Microsystem and Information Technology, Chinese Academy of Science, Shanghai 200050, People's Republic of China

²University of Chinese Academy of Sciences, Beijing 100049, People's Republic of China

³Department of Physics, Laboratory of Advanced Materials, and Surface Physics Laboratory (National Key Laboratory), Fudan University, Shanghai 200438, People's Republic of China

⁴School of Physical Science and Technology, ShanghaiTech University, Shanghai 201210, People's Republic of China



(Received 16 June 2021; revised 2 November 2021; accepted 18 November 2021; published 7 December 2021)

Topological superconductors are materials in which superconductivity is closely entangled with topological electronic states. This provides a promising route to create Majorana bound states that are of fundamental importance to fault-tolerant quantum computation. In this paper, the recently discovered superconductor CaBi₂ has been identified as a three-dimensional topological material. Spin-split topological surface states intersecting the Fermi energy are experimentally observed via spin- and angle-resolved photoemission spectroscopy. They are highly consistent with theoretical calculations. Furthermore, the layer-locked spin structure of CaBi₂ is revealed via the layer-resolved spin texture analysis. These results unambiguously reveal the topological properties of the spin-polarized electronic structure in CaBi₂ and provide important clues in the search for Majorana fermions in Bi-based topological superconductors.

DOI: [10.1103/PhysRevB.104.245112](https://doi.org/10.1103/PhysRevB.104.245112)

I. INTRODUCTION

Topological superconductors have stimulated extensive research because of the coexistence of topological and superconducting states where Cooper pairs are formed by spin-polarized topological surface states. They are promising materials for the formation of Majorana bound states or fermions, which are of fundamental importance as potential quantum bytes for fault-tolerant quantum computation [1,2].

To create Majorana fermions, significant effort has been devoted to induce a superconducting transition in a topological insulator through doping or intercalation, such as Cu-intercalated Bi₂Se₃ [3–6] and In-doped SnTe [7]. A zero-bias conductance peak in the superconducting gap has been observed in such systems with scanning tunneling spectroscopy, suggesting a possible approach to create Majorana fermions [6,7]. In addition, recent theoretical predictions suggest the fabrication of a topological and superconductor heterostructure where Cooper pairs can tunnel into topological surface states because of the proximity effect would form Majorana bound states at a vortice [8]. The existence of a Majorana zero mode in a topological insulator heterostructure, such as Bi₂Te₃/NbSe₂, was confirmed by a series of evidences with scanning tunneling microscopy [9–11]. However, the realization of Majorana fermions largely depends on the thickness of the Bi₂Te₃ layer as well as the high quality of the

interface. This remarkably increases the difficulty for device fabrication.

The coexistence of superconducting and topological surface states in a single crystal provides a new route to create Majorana fermions [1,2]. Until now, topological states were investigated in a few superconducting systems [12–20], such as β -PdBi₂ [21–24] and FeTe_{0.55}Se_{0.45} [25–27] in which robust zero-bias conductance peaks were also observed at vortex cores. Nevertheless, the interplay between topological states and superconductivity in a single crystal remains unclear and needs further theoretical and experimental characterizations.

Recently, a layered crystal of CaBi₂ has been identified as a superconductor with a transition temperature at 2 K [28]. Theoretical calculations suggest that the strong spin-orbit coupling (SOC) in CaBi₂ affects the topology of the Fermi surface and modifies the electron-phonon coupling parameter that is of fundamental importance to superconductivity [29]. However, the electronic band structures of superconducting CaBi₂ have not yet been analyzed in detail. Thus, the underlying mechanism of topological electronic states in CaBi₂ is still lacking, which prevents an understanding of the interplay between the band topology and the superconductivity.

Here, we present a comprehensive examination of the topological properties of superconducting CaBi₂ crystals. We found that the layered CaBi₂ crystal possesses a topologically nontrivial electronic structure where band inversion occurs at the Γ point because of SO interactions. Additionally, its strong topological property was, subsequently, identified by calculations of \mathbb{Z}_2 invariants, suggesting the existence of topological surface states. The CaBi₂ electronic band structures were experimentally probed with spin- and angle-resolved

*qiaoshan@mail.sim.ac.cn

†yemao@mail.sim.ac.cn

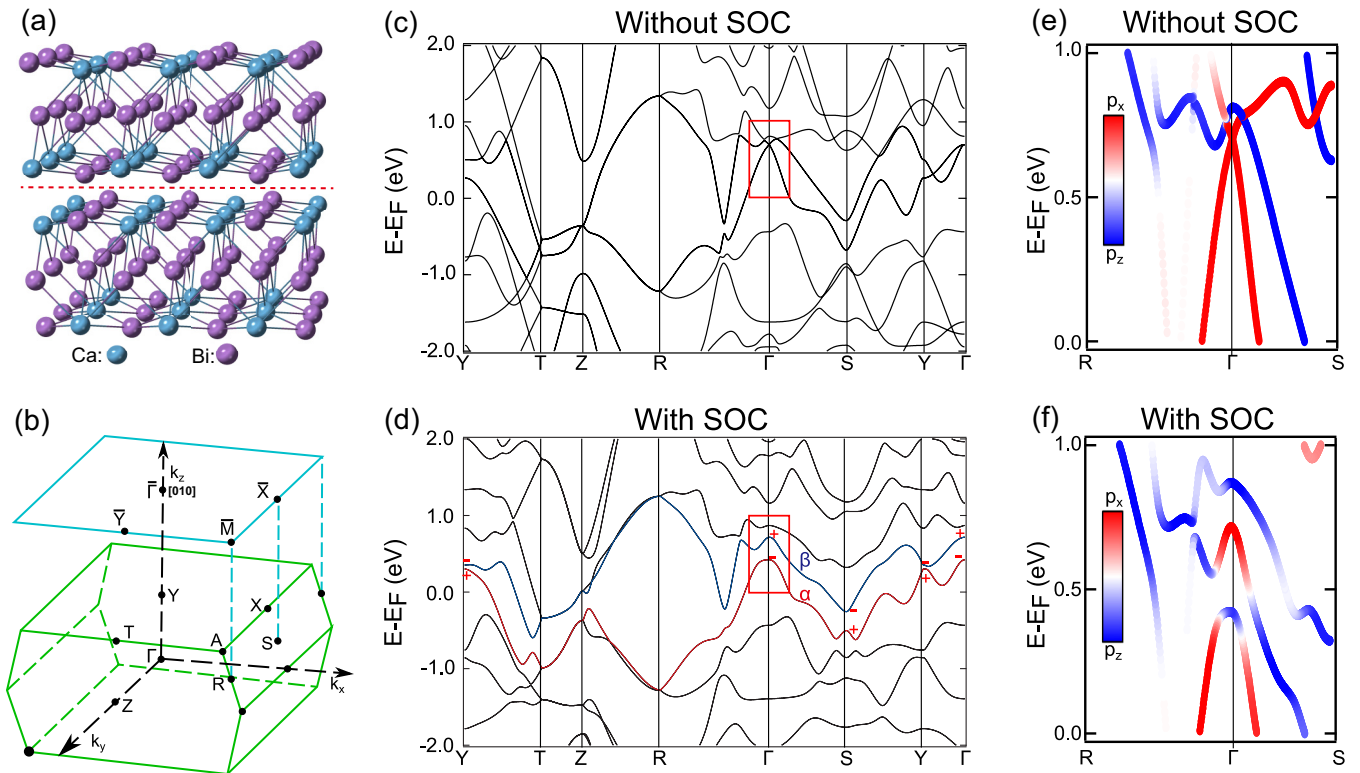


FIG. 1. Crystal structures and band topology of CaBi_2 . (a) Atomic structure of layered CaBi_2 . (b) Surface and bulk Brillouin zones of CaBi_2 . (c) First-principles calculations of bulk band structures along high-symmetry directions without spin-orbit interactions where the band overlap at the Γ point is indicated by a red rectangle. (d) Calculated bulk band structures with spin-orbit interactions. The parity eigenvalues at the time-reversal symmetry points are indicated explicitly. (e) and (f) Contributions from p_z (blue) and p_x (red) orbitals of Bi $6p$ without and with SOC in the region where band inversion is indicated by red rectangles in (c) and (d), respectively.

photoemission spectroscopy (SARPES). It is unambiguously unmasked that the spin-split topological surface states intersect the Fermi surface, which is required for topological superconductors. In addition, the bulk electronic states exhibit nonzero spin polarization in surface-sensitive SARPES because of layer-dependent spin locking revealed by slab calculations. The spin-polarized electrons in both surface and bulk states in superconducting CaBi_2 revealed here may stimulate further research on Majorana fermions in Bi-based superconductors, which will remarkably facilitate the realization of fault-tolerant quantum computations.

II. EXPERIMENTS AND METHODS

Single crystals of CaBi_2 were grown using a Bi self-flux method [28]. Calcium pieces (99.99%) and bismuth granules (99.99%) were weighted and mixed at the Ca:Bi molar ratio of 3:17 in an Ar-filled glovebox (H_2O , $\text{O}_2 < 0.1$ ppm). The mixture was placed in an alumina crucible and then sealed in a quartz ampule under high vacuum. The ampule was heated 823 K and maintained for 6 h and then gradually cooled to 583 K at a rate of 3 K/h. At 583 K, the quartz ampule was removed from the furnace and centrifuged to separate the crystals from the flux. ARPES was performed at the BL03U beamline of the Shanghai Synchrotron Radiation Facility with a hemispherical electron-energy analyzer (Scienta-Omicron DA30) [30,31]. SARPES was performed with a home-made image-type spin detector with a 0.25 Sherman function; it

was attached to a hemispherical electron-energy analyzer [32]. SARPES spectra were acquired with a monochromatic He discharge ($\text{He I}\alpha$, 21.2-eV) excitation source with a total instrumental energy resolution of 30 meV. Electronic band structure calculations were performed in the framework of density functional theory using the Vienna *ab initio* simulation package [33–35]. Surface electronic states and the \mathbb{Z}_2 topological index were calculated by constructing localized Wannier functions [36,37] with the WANNIERTOOLS package [38].

III. RESULTS

A. Band topology of CaBi_2

According to previous theoretical and experimental reports [28,29,39], CaBi_2 has an orthorhombic lattice structure, which belongs to the $Cmcm$ nonsymmorphic symmetry group (No. 63). The layered CaBi_2 crystal structure is shown in Fig. 1(a) where the Bi layer is sandwiched between two corrugated Ca-Bi layers. These trilayers are stacked along the [010] direction. The natural cleavage plane is between the upper and the lower Ca-Bi layers as indicated by the red dashed line. The projected surface Brillouin zone is shown in Fig. 1(b), according to the [010] direction of the experimentally cleaved surface. The high-symmetry points are labeled.

Calculated bulk electronic band structures without SOC along high-symmetry directions are shown in Fig. 1(c). We focused on bands near the Fermi energy. Band overlap occurs in the vicinity of the Γ point above the Fermi energy as indicated

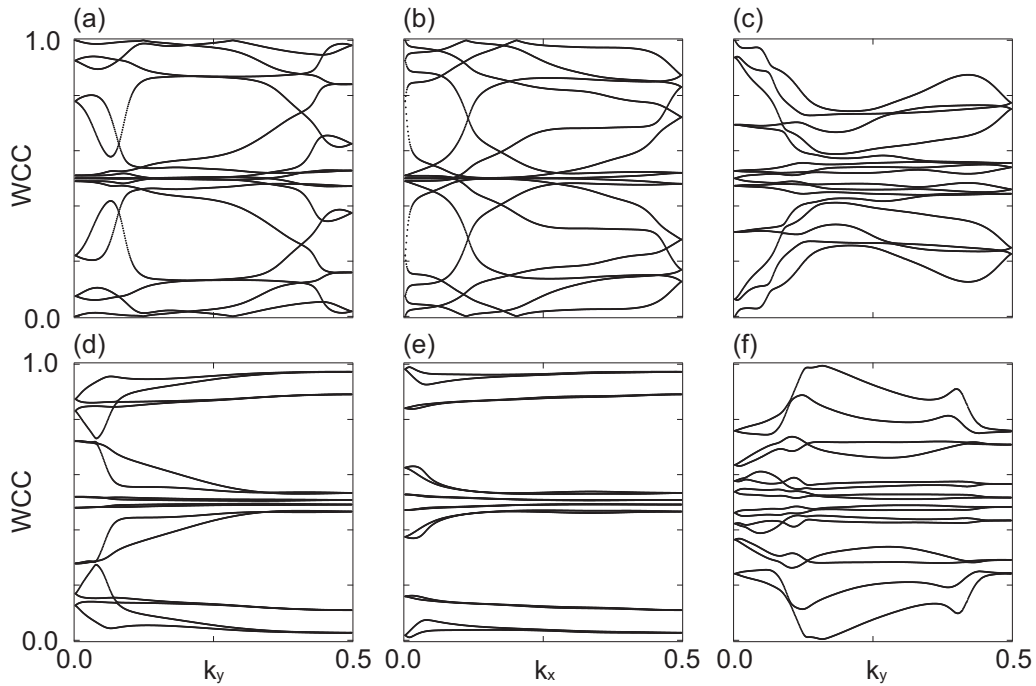


FIG. 2. Wannier charge centers evolution for the time-reversal invariant planes of CaBi_2 . (a) $\mathbb{Z}_2 = 1$ for $k_x = 0$. (b) $\mathbb{Z}_2 = 1$ for $k_y = 0$. (c) $\mathbb{Z}_2 = 1$ for $k_z = 0$. (d) $\mathbb{Z}_2 = 0$ for $k_x = \pi/a$. (e) $\mathbb{Z}_2 = 0$ for $k_y = \pi/b$. (f) $\mathbb{Z}_2 = 0$ for $k_z = \pi/c$.

by a red rectangle. When SOC is included, a gap-opening occurs between the valance (α) and conduction (β) bands, which are, respectively, plotted in blue and red in Fig. 1(d). Meanwhile, the parity eigenvalues at the time-reversal symmetry points are indicated explicitly. The opposite parity at the Γ point is shown relative to those at the S and Y points, suggesting the occurrence of band inversion in the center of the Brillouin zone. To gain a deeper insight into the mechanism of the band inversion, the orbital contributions to the electronic states near the Γ point without and with SOC were plotted in Figs. 1(e) and 1(f), respectively. Electronic states near the Fermi energy are mainly derived from Bi p_z and p_x orbitals between which the band inversion is clearly observed at 0.5 eV above the Fermi energy.

To confirm the CaBi_2 topological classification, four \mathbb{Z}_2 topological invariants (v_0 , v_1 , v_2 , and v_3) were computed based on the Wannier charge-centers method [40–42], where v_0 is a strong topological index and (v_1 , v_2 , and v_3) are three weak topological indices [43]. Such a \mathbb{Z}_2 number can be obtained via Wannier charge centers (WCCs) calculations on six time-reversal invariant planes (k_x , k_y , and $k_z = 0, \pi$) making use of the WANNIERTOOLS package [38]. Based on the band calculation in Fig. 1(d), the α and β bands are continuously gapped throughout the Brillouin zone with each other, which meets the condition of \mathbb{Z}_2 topological invariants calculations. All the bands below β have been taken into account to calculate the WCCs, and the computed results are shown in Fig. 2, which suggest that the \mathbb{Z}_2 indices are 1 for k_x , k_y , $k_z = 0$ planes, whereas zero for k_x , k_y , and $k_z = \pi$ planes. The results show that \mathbb{Z}_2 topological invariants of CaBi_2 are (1, 000), categorizing CaBi_2 as a strong topological material [40] and suggesting the existence of topological surface states.

B. Electronic band structures of CaBi_2

The topological properties in CaBi_2 were investigated with ARPES. Although CaBi_2 has a layered crystal structure, the layered coupling along the [010] direction is not negligible. Figure 3 shows detailed photon-energy-dependent electronic states on the k_x - k_z planes at different binding energies, which were obtained via changing the photon energy from 89 to 158 eV. As can be seen, electronic states along the k_z direction exhibit periodic dispersions at different constant-energy contours, which are shown in Figs. 3(a)–3(c). The holelike pocket periodically appears at the 0.45-eV binding energy below E_F , which is consistent well with band calculations in Fig. 3(d), thus, the high-symmetry momentum positions (Γ and Y) are precisely identified.

Moreover, an inner potential $V_0 = 26$ eV can be deduced with the free-electron final-state model via the best fit to the periodic variation with the lattice constant $b = 17.081$ Å. Then it can be calculated that $h\nu = 31, 54$ eV corresponds to the Brillouin-zone center whereas $h\nu = 22, 42$ eV is close to the Y point during the range of low photon energy.

Figure 4(a) shows a three-dimensional view of the band dispersions of CaBi_2 probed with a 53-eV photon energy where the excited electronic states are close to the Brillouin-zone center along the k_z direction. According to the bulk band calculations in Fig. 1(d), the band inversion occurs along the Γ - S direction, which is projected into the surface Brillouin zone as the experimentally measured $\bar{\Gamma}$ - \bar{X} direction [Fig. 4(b)]. For a better comparison, the calculated bulk bands (α and β) along the Γ - X direction are superimposed with the ARPES spectrum as shown in Fig. 4(b). The electronic states indicated by green arrows are suggested surface states that pass through the energy gap of the inverted bulk bands α and β .

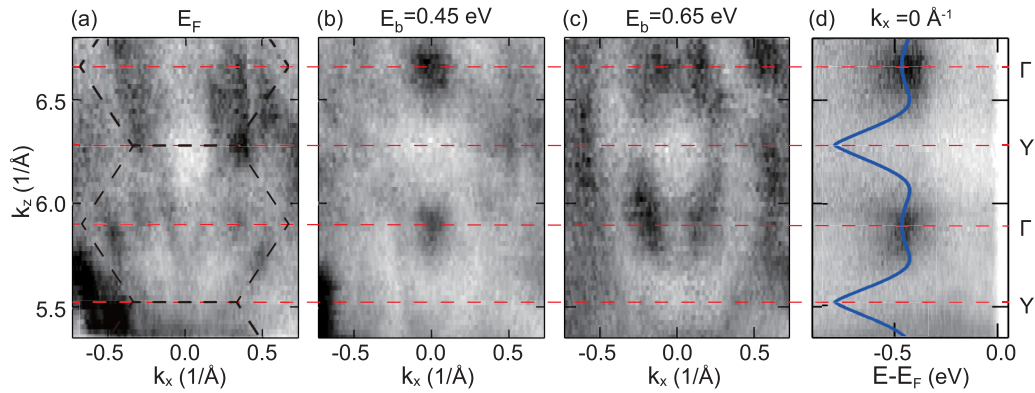


FIG. 3. Band structures along the k_z direction probed by continuously varied photon energy. (a)–(c) Constant-energy contours of the photoemission spectra along the k_z - k_x sheet at different binding energies in which the Brillouin zone is indicated by the dashed hexagons. (d) Band dispersions along the k_z direction at $k_x = 0 \text{ \AA}^{-1}$ in which the related band calculations along the Γ - Y direction are superimposed with the blue lines.

As mentioned above, the strong SOC is a key factor to induce the band inversion of α and β bands, although the inverted bands are located above the Fermi energy, which cannot be observed through the ARPES measurement. Using the WANNIERTOOLS package [38], we performed first-principles simulations to calculate the surface and bulk states of CaBi_2 along the \bar{X} - $\bar{\Gamma}$ - \bar{X} direction without and with SOC, respectively. The computed results are shown in Figs. 4(c) and 4(d). As can be seen, the dispersion of bulk states changes a lot when SOC is included where the gap opening at binding energy of 0.5 and 1.5 eV in Fig. 4(d) is visible. Meanwhile, two topological surface states (TSSs) that intersect the Fermi energy and connect the valence band (α) to the conduction band (β) agree well with the experimentally observed band dispersion, which are indicated by red arrows. Such TSSs that originate from the band inversion at the Γ point between the p_x and the p_z electrons were also found in PdTe_2 and NiTe_2 [44,45] where the derived surface states stretch from the vicinity of the $\bar{\Gamma}$ point into the Brillouin-zone boundary. This indicates that the generation of such topological states is not restricted to CaBi_2 , but a common characteristic of p -electron systems with strong SO interactions. Moreover, a Rashba-like surface state occurs at the \bar{X} point near the Fermi energy, which has been observed in the experimental spectrum. Nevertheless, since most part of such Rashba-like surface states are located above the Fermi energy, it cannot be clearly resolved by the ARPES method in the present paper.

C. Spin-polarized topological surface states

To clarify the surface nature of topological states, the photon-energy-dependent ARPES measurement has been performed via changing the photon energy from 47 to 62 eV along the $\bar{\Gamma}$ - \bar{X} - $\bar{\Gamma}$ direction, which has covered nearly one bulk Brillouin zone along the k_z direction. The surface state is clearly observed at such an energy range as shown in Fig. 5(a). TSS2 is indicated by the blue arrows and traced by the blue dashed line on the $h\nu$ - k_x plane. As can be seen, TSS2 exhibits as a straight line in the $h\nu$ - k_x spectrum and shows negligible dispersion along the k_z direction, which evidences a surface state nature of TSS2. In addition, the α band indicated by the

red arrows shows a broadening shape and a dispersive feature at the Γ point along the k_z direction, which proved its bulk state nature.

To observe such TSSs more clearly, photon energy of $h\nu = 21 \text{ eV}$ was used for better energy and momentum resolution. The excited electronic states are close to the boundary of the Brillouin zone (Y point) along the k_z direction [Fig. 5(c)]. TSS1 extends from the Fermi energy to the 0.2-eV binding energy, and TSS2 intersects with TSS1 near the Fermi energy, extending to the \bar{X} point of the α band. This is very consistent with the surface-state calculations in Fig. 4(d). The calculated spin-polarized electronic states along the \bar{X} - $\bar{\Gamma}$ - \bar{X} direction close to the Fermi energy are plotted in Fig. 5(d). It suggests that the electrons in these two TSSs have opposite spin polarizations. The spin directions are perpendicular to that of the electron momentum, indicating a spin-momentum locked texture. However, the calculated electronic states around the $\bar{\Gamma}$ point near the Fermi energy have a relatively weak spectrum weight in Fig. 5(c). It may be affected by the photoemission process due to the horizontal-polarized synchrotron radiation light.

The SARPES measurement was performed with a home-made image-type spin polarimeter based on the very-low-energy-electron diffraction mechanism [5], which is attached to a hemispherical electron energy analyzer as schematically shown in Fig. 6(a). The two-dimensional images of band dispersions formed on the exit plane of the hemispherical analyzer are transferred to an oxygen-passivated ferromagnetic $\text{Fe}(001)$ - $p(1 \times 1)$ - O target, realizing parallel detecting with 78 and 87 channels in angular- and energy-directions, respectively [26]. The spin texture was experimentally verified by spin-resolved measurements using monochromatic 21-eV photons. Figures 6(b) and 6(c) exhibit photoemission spectra with intensities and spin polarization along the $\bar{\Gamma}$ - \bar{X} direction, respectively. The experimentally identified spin polarization of TSS1 adjacent to the Fermi energy is consistent with our calculations where it connects to other surface states with opposite spin polarization at the higher binding energy of 0.2 eV. Unfortunately, the TSS2 intensity is relatively weak in the photoemission spectrum [Fig. 6(b)] because of the He-lamp 21-eV photon source. According to the spin calculations in

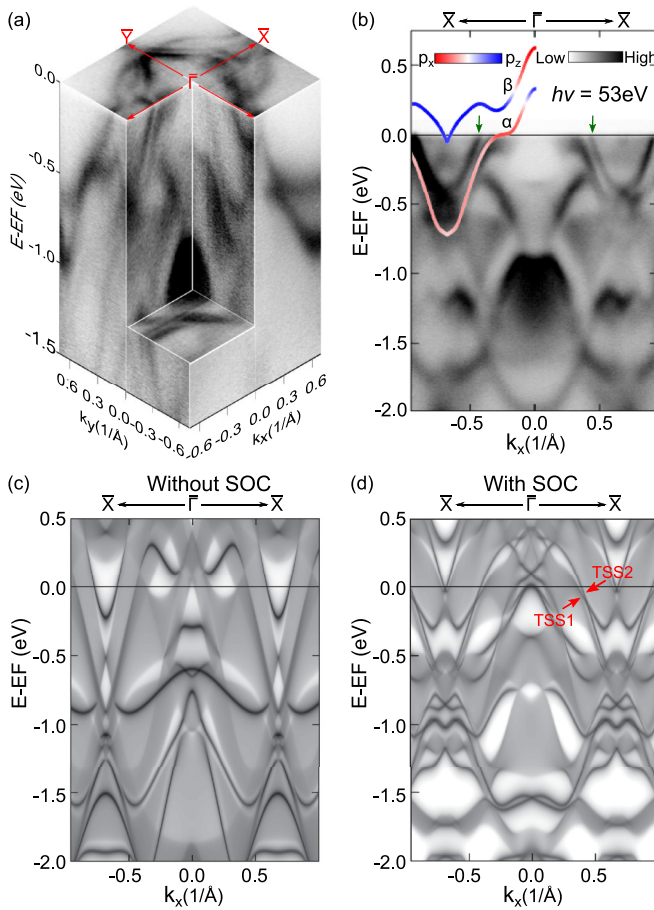


FIG. 4. Electronic states around the Γ point of the Brillouin zone. (a) Electronic band structures of CaBi_2 measured with 53-eV photon energy where the probed electronic states are close to the center of the Brillouin zone in the k_z direction. (b) Measured band dispersions of CaBi_2 along the $\bar{X}-\Gamma-\bar{X}$ direction where the calculations of inverted α - and β -bulk bands are superimposed. Surface states located between the α - and the β -bulk bands are marked by green arrows. (c) Calculated electronic states along the $\bar{X}-\Gamma-\bar{X}$ direction without SOC. (d) Calculated electronic states along the $\bar{X}-\Gamma-\bar{X}$ direction with SOC where the topological surface states transfer across the Fermi surface, indicated by two red arrows.

Fig. 5(d), bulk states at 0.2-eV binding energy are adjacent to TSS2 with the same spin orientation. As a result, it appears that TSS2 is integrated into the experimentally observed bulk states [Fig. 6(c)].

The energy distribution curve is shown in Fig. 6(d), which is obtained by integration of the intensity in the green dashed box denoted in (c). The spin polarization of TSS1 can be clearly resolved in the vicinity of the Fermi energy, which is indicated by the red arrow. It is worth noting that the measured spin polarization of TSS1 is low (about 10%) because the background intensity of the photoemission spectrum is relatively high, which decreased the experimentally measured spin polarization. Despite this, the spin orientation of TSS1 is correctly identified, which indicates the spin-momentum-locked texture. In addition, the electronic states along the $\bar{M}-\bar{X}-\bar{M}$ direction has been investigated by previous work, which is focused on the band topology at the \bar{X} point at the

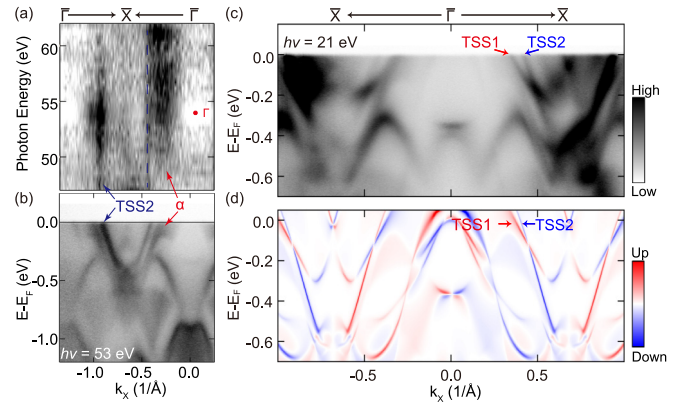


FIG. 5. Topologically nontrivial states intersecting the Fermi energy in CaBi_2 . (a) Constant-energy contours of the photoemission spectra along the $h\nu-k_x$ sheet at the Fermi energy. (b) Electronic band dispersions along the $\bar{X}-\Gamma-\bar{X}$ direction obtained with the photon energy of 53 eV. (c) Electronic band structures of CaBi_2 along the $\bar{X}-\Gamma-\bar{X}$ direction measured with 21-eV photons. Two TSSs passing through the Fermi energy are observed as indicated by red and blue arrows. (d) Calculated spin-polarized electronic states corresponding to the angle-resolved photoemission spectroscopy feature in (c).

binding energy of 0.53 eV below the Fermi energy [46]. For the electronic states at the \bar{X} point, the band gap occurs, but the topological surface states are not clearly observed in Figs. 4(b) and 5(c), which may need further experimental and theoretical investigations.

D. Layer-locked spin texture

Furthermore, the measured spin polarizations in the bulk states are nonzero, although the spin in the bulk states should be compensated due to the space-inversion symmetry of the whole CaBi_2 crystal. However, recent theoretical and experimental works suggest that the dipole field in the centrosymmetric crystal may induce layer-locked spin-polarized electronic states because of the strong SOC [47,48]. With the SARPES surface sensitivity, the contribution to the projected spin polarization from the first layer will be enhanced relative to those from deeper layers. This results in the experimentally observed spin polarization in the bulk states [49–51].

We constructed a 10-unit-cell supercell for slab calculations to examine layer-dependent spin polarization in CaBi_2 . Figure 7 shows that the atoms in each layer have sizable spin polarizations where the calculated spin polarization of the bulk states locked on the first Bi layer is consistent with the experimental observation in Fig. 6(c). Although the electronic states near the Fermi energy are mainly contributed from the Bi 6*p* orbitals, the layer-locked spin-polarized states of Ca atoms also appear because of Ca and Bi hybridizations. This is shown in Figs. 7(c) and 7(f), which corresponds to Ca layers.

Recent theoretical and experimental works suggest that the strong SO interactions of Bi can affect the strength of electron-phonon coupling in Bi-based superconductors [28,29,52,53], even remarkably enhancing the superconducting temperatures of the KBi_2 and SrBi_3 systems [54–57]. CaBi_2 is similar to

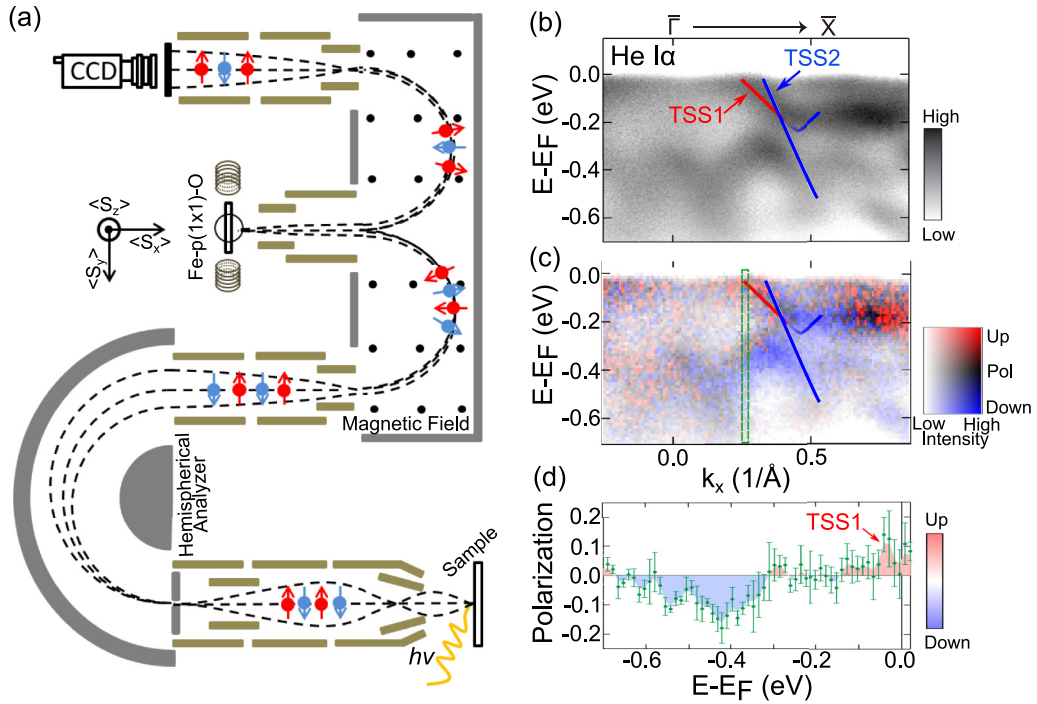


FIG. 6. Spin-resolved surface electronic states of CaBi_2 . (a) Schematic of the image-type SARPES. (b) and (c) Spin-resolved photoemission spectra measured with 21-eV photons where the red and blue lines are visual guides based on the measured band dispersions. (d) Energy distribution curves obtained by integration of the intensity in the green dashed boxes denoted in (c).

these Bi-based superconducting materials where Bi $6p$ SO interactions play a key role in inducing spin-split TSSs and the layer-locked spin texture. Hence, these spin-polarized states close to the Fermi energy may be able to form superconducting triplet states. This would change the superconductivity relative to that derived from spin-singlet states. Therefore, a new route may be provided to characterize topological superconducting properties in CaBi_2 and other Bi-based superconductors.

IV. CONCLUSION

To summarize, the superconductor CaBi_2 was identified as a three-dimensional topological material because of the band inversion of Bi p_z and p_x orbitals. TSSs were clearly resolved with SARPES, which intersect the Fermi energy with a spin-momentum-locked texture. Moreover, the calculated electronic bulk states for each layer exhibit nonzero spin polarization that suggests a layer-locked spin texture in

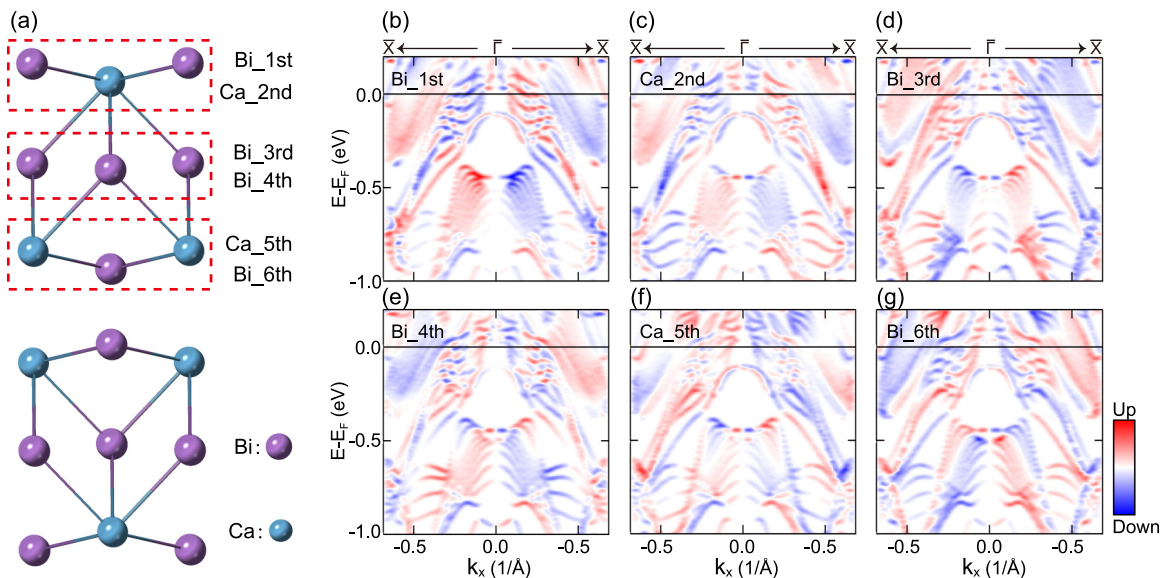


FIG. 7. Layer-resolved spin texture of CaBi_2 by slab calculation. (a) Layered CaBi_2 crystal structure where the first six layers are labeled. (b)–(g) Calculated layer-dependent spin polarization contributed by each of the six layers.

CaBi₂. The spin texture is manifested by the surface-sensitive SARPES measurements that show finite spin polarization from observed bulk states. The spin-polarized electronic states are all derived from strong SOC in Bi that has a large effect on previously reported superconducting temperatures in Bi-based materials. Therefore, the confirmation of such topologically nontrivial electronic states in superconducting CaBi₂ may provide a route to study the interplay between band topology and superconductivity. This will stimulate further research to explore Majorana bound states in Bi-based superconductors.

ACKNOWLEDGMENTS

This work was supported by the National Key R&D Program of China (Grant No. 2017YFA0305400) and the Natural Science Foundation of China (Grants No. U1632266, No. U2032207, No. 11927807, and No. U2032208). The ARPES experiments were performed with the approval of the Proposal Assessing Committee of SiP-ME² platform project (Proposal No. 11227902). We acknowledge Q.-S. Wu for the development of the user-oriented WANNIERTOOLS package.

-
- [1] M. Leijnse and K. Flensberg, *Semicond. Sci. Technol.* **27**, 124003 (2012).
- [2] M. Sato and S. Fujimoto, *J. Phys. Soc. Jpn.* **85**, 072001 (2016).
- [3] Y. S. Hor, A. J. Williams, J. G. Checkelsky, P. Roushan, J. Seo, Q. Xu, H. W. Zandbergen, A. Yazdani, N. P. Ong, and R. J. Cava, *Phys. Rev. Lett.* **104**, 057001 (2010).
- [4] L. Fu and E. Berg, *Phys. Rev. Lett.* **105**, 097001 (2010).
- [5] M. Kriener, K. Segawa, Z. Ren, S. Sasaki, and Y. Ando, *Phys. Rev. Lett.* **106**, 127004 (2011).
- [6] S. Sasaki, M. Kriener, K. Segawa, K. Yada, Y. Tanaka, M. Sato, and Y. Ando, *Phys. Rev. Lett.* **107**, 217001 (2011).
- [7] S. Sasaki, Z. Ren, A. A. Taskin, K. Segawa, L. Fu, and Y. Ando, *Phys. Rev. Lett.* **109**, 217004 (2012).
- [8] L. Fu and C. L. Kane, *Phys. Rev. Lett.* **100**, 096407 (2008).
- [9] J. P. Xu, C. Liu, M. X. Wang, J. F. Ge, Z. L. Liu, X. J. Yang, Y. Chen, Y. Liu, Z. A. Xu, C. L. Gao, D. Qian, F. C. Zhang, and J. F. Jia, *Phys. Rev. Lett.* **112**, 217001 (2014).
- [10] J. P. Xu, M. X. Wang, Z. L. Liu, J. F. Ge, X. J. Yang, C. H. Liu, Z. A. Xu, D. D. Guan, C. L. Gao, D. Qian, Y. Liu, Q. H. Wang, F. C. Zhang, Q. K. Xue, and J. F. Jia, *Phys. Rev. Lett.* **114**, 017001 (2015).
- [11] H. H. Sun, K. W. Zhang, L. H. Hu, C. Li, G. Y. Wang, H. Y. Ma, Z. A. Xu, C. L. Gao, D. D. Guan, Y. Y. Li, C. H. Liu, D. Qian, Y. Zhou, L. Fu, S. C. Li, F. C. Zhang, and J. F. Jia, *Phys. Rev. Lett.* **116**, 257003 (2016).
- [12] S. Y. Guan, P. J. Chen, M. W. Chu, R. Sankar, F. Chou, H. T. Jeng, C. S. Chang, and T. M. Chuang, *Sci. Adv.* **2**, e1600894 (2016).
- [13] G. Bian, T. R. Chang, R. Sankar, S. Y. Xu, H. Zheng, T. Neupert, C. K. Chiu, S. M. Huang, G. Chang, I. Belopolski, D. S. Sanchez, M. Neupane, N. Alidoust, C. Liu, B. K. Wang, C. C. Lee, H. T. Jeng, C. L. Zhang, Z. J. Yuan, S. Jia *et al.*, *Nat. Commun.* **7**, 10556 (2016).
- [14] T. Le, Y. Sun, H. K. Jin, L. Che, L. Yin, J. Li, G. Pang, C. Xu, L. Zhao, S. Kittaka, T. Sakakibara, K. Machida, R. Sankar, H. Q. Yuan, G. F. Chen, X. F. Xu, S. Y. Li, Y. Zhou, and X. Lu, *Sci. Bull.* **65**, 1349 (2020).
- [15] P. Zhang, Z. Wang, X. Wu, K. Yaji, Y. Ishida, Y. Kohama, G. Dai, Y. Sun, C. Bareille, K. Kuroda, T. Kondo, K. Okazaki, K. Kindo, X. C. Wang, C. Q. Jin, J. P. Hu, R. Thomale, K. Sumida, S. L. Wu, K. Miyamoto *et al.*, *Nat. Phys.* **15**, 41 (2019).
- [16] Q. Liu, C. Chen, T. Zhang, R. Peng, Y.-J. Yan, C.-H.-P. Wen, X. Lou, Y.-L. Huang, J.-P. Tian, X.-L. Dong, G.-W. Wang, W.-C. Bao, Q.-H. Wang, Z.-P. Yin, Z.-X. Zhao, and D.-L. Feng, *Phys. Rev. X* **8**, 041056 (2018).
- [17] Y. Yuan, J. Pan, X. Wang, Y. Fang, C. Song, L. Wang, K. He, X. Ma, H. Zhang, F. Huang, W. Li, and Q. K. Xue, *Nat. Phys.* **15**, 1046 (2019).
- [18] L. S. Wang, Y. Q. Fang, Y. Y. Huang, E. J. Cheng, J. M. Ni, B. L. Pan, Y. Xu, F. Q. Huang, and S. Y. Li, *Phys. Rev. B* **102**, 024523 (2020).
- [19] C. Chen, A. Liang, S. Liu, S. Nie, J. Huang, M. Wang, Y. Li, D. Pei, H. Yang, H. Zheng, Y. Zhang, D. H. Lu, M. Hashimoto, A. Barinov, C. Jozwiak, A. Bostwick, E. Rotenberg, X. F. Kou, L. X. Yang, Y. F. Guo, Z. J. Wang *et al.*, *Matter* **3**, 2055 (2020).
- [20] B. R. Ortiz, S. M. L. Teicher, Y. Hu, J. L. Zuo, P. M. Sarte, E. C. Schueller, A. M. Milinda Abeykoon, M. J. Krogstad, S. Rosenkranz, R. Osborn, R. Seshadri, L. Balents, J. He, and S. D. Wilson, *Phys. Rev. Lett.* **125**, 247002 (2020).
- [21] M. Sakano, K. Okawa, M. Kanou, H. Sanjo, T. Okuda, T. Sasagawa, and K. Ishizaka, *Nat. Commun.* **6**, 8595 (2015).
- [22] Y. F. Lv, W. L. Wang, Y. M. Zhang, H. Ding, W. Li, L. Wang, K. He, C. L. Song, X. C. Ma, and Q. K. Xue, *Sci. Bull.* **62**, 852 (2017).
- [23] Y. Li, X. Xu, M. H. Lee, M. W. Chu, and C. Chien, *Science* **366**, 238 (2019).
- [24] J. Y. Guan, L. Kong, L. Q. Zhou, Y. G. Zhong, H. Li, H. J. Liu, C. Y. Tang, D. Y. Yan, F. Z. Yang, Y. B. Huang, Y. G. Shi, T. Qian, H. M. Weng, Y. J. Sun, and H. Ding, *Sci. Bull.* **64**, 1215 (2019).
- [25] P. Zhang, K. Yaji, T. Hashimoto, Y. Ota, T. Kondo, K. Okazaki, Z. Wang, J. Wen, G. Gu, H. Ding, and S. Shin, *Science* **360**, 182 (2018).
- [26] D. Wang, L. Kong, P. Fan, H. Chen, S. Zhu, W. Liu, L. Cao, Y. Sun, S. Du, J. Schneeloch, R. Zhong, G. Gu, L. Fu, H. Ding, and H. J. Gao, *Science* **362**, 333 (2018).
- [27] S. Zhu, L. Kong, L. Cao, H. Chen, M. Papaj, S. Du, Y. Xing, W. Liu, D. Wang, C. Shen, F. Z. Yang, J. Schneeloch, R. D. Zhong, G. D. Gu, L. Fu, Y. Y. Zhang, H. Ding, and H. J. Gao, *Science* **367**, 189 (2020).
- [28] M. J. Winiarski, B. Wiendlocha, S. Gob, S. K. Kushwaha, P. Winiewski, D. Kaczorowski, J. D. Thompson, R. J. Cava, and T. Klimczuk, *Phys. Chem. Chem. Phys.* **18**, 21737 (2016).
- [29] S. Golab and B. Wiendlocha, *Phys. Rev. B* **99**, 104520 (2019).
- [30] Y. C. Yang, Z. T. Liu, J. S. Liu, Z. H. Liu, W. L. Liu, X. L. Lu, H. P. Mei, A. Li, M. Ye, S. Qiao, and D. W. Shen, *Nucl. Sci. Technol.* **32**, 1 (2021).
- [31] Z. P. Sun, Z. H. Liu, Z. T. Liu, W. L. Liu, F. Y. Zhang, D. W. Shen, M. Ye, and S. Qiao, *J. Synchrotron Radiat.* **27**, 1388 (2020).

- [32] F. Ji, T. Shi, M. Ye, W. Wan, Z. Liu, J. Wang, T. Xu, and S. Qiao, *Phys. Rev. Lett.* **116**, 177601 (2016).
- [33] G. Kresse and J. Hafner, *Phys. Rev. B* **47**, 558 (1993).
- [34] G. Kresse and J. Furthmuller, *Phys. Rev. B* **54**, 11169 (1996).
- [35] G. Kresse and D. Joubert, *Phys. Rev. B* **59**, 1758 (1999).
- [36] N. Marzari and D. Vanderbilt, *Phys. Rev. B* **56**, 12847 (1997).
- [37] A. A. Mostofi, J. R. Yates, Y. S. Lee, I. Souza, D. Vanderbilt, and N. Marzari, *Comput. Phys. Commun.* **178**, 685 (2008).
- [38] Q. S. Wu, S. Zhang, H. F. Song, M. Troyer, and A. A. Soluyanov, *Comput. Phys. Commun.* **224**, 405 (2018).
- [39] Y. Lyu, H. Yuan, S. Daneshmandi, S. Huyan, and C. W. Chu, *J. Phys. Chem. Lett.* **11**, 4385 (2020).
- [40] L. Fu and C. L. Kane, *Phys. Rev. B* **76**, 045302 (2007).
- [41] A. A. Soluyanov and D. Vanderbilt, *Phys. Rev. B* **83**, 235401 (2011).
- [42] H. M. Weng, X. Dai, and Z. Fang, *MRS Bull.* **39**, 849 (2014).
- [43] L. Fu, C. L. Kane, and E. J. Mele, *Phys. Rev. Lett.* **98**, 106803 (2007).
- [44] O. J. Clark, M. J. Neat, K. Okawa, L. Bawden, I. Markovic, F. Mazzola, J. Feng, V. Sunko, J. M. Riley, W. Meevasana, J. Fujii, I. Vobornik, T. K. Kim, M. Hoesch, T. Sasagawa, P. Wahl, M. S. Bahramy, and P. D. C. King, *Phys. Rev. Lett.* **120**, 156401 (2018).
- [45] S. Mukherjee, S. W. Jung, S. F. Weber, C. Xu, D. Qian, X. Xu, P. K. Biswas, T. K. Kim, L. C. Chapon, M. D. Watson, J. B. Neaton, and C. Cacho, *Sci. Rep.* **10**, 12957 (2020).
- [46] G. Dhakal, M. M. Hosen, A. Ghosh, C. Lane, K. Gornicka, M. J. Winarski, K. Dimitri, F. Kabir, C. Sims, S. Regmi, W. Neff, L. Persaud, Y. Liu, D. Kaczorowski, J.-X. Zhu, T. Klimczuk, and M. Neupane, [arXiv:1911.08519](https://arxiv.org/abs/1911.08519).
- [47] X. Zhang, Q. Liu, J. W. Luo, A. J. Freeman, and A. Zunger, *Nat. Phys.* **10**, 387 (2014).
- [48] J. M. Riley, F. Mazzola, M. Dendzik, M. Michiardi, T. Takayama, L. Bawden, C. Granerd, M. Leandersson, T. Balasubramanian, and M. Hoesch, *Nat. Phys.* **10**, 835 (2014).
- [49] W. Yao, E. Wang, H. Huang, K. Deng, M. Yan, K. Zhang, K. Miyamoto, T. Okuda, L. Li, Y. Wang, H. J. Gao, C. X. Liu, W. H. Duan, and S. Y. Zhou, *Nat. Commun.* **8**, 14216 (2017).
- [50] T. Xu, B. T. Wang, M. Wang, Q. Jiang, X. P. Shen, B. Gao, M. Ye, and S. Qiao, *Phys. Rev. B* **100**, 161109 (2019).
- [51] Q. Jiang, W. Xia, T. Xu, W. Liu, X. Shen, Y. Guo, M. Ye, and S. Qiao, *J. Electron Spectrosc. Relat. Phenom.* **238**, 146868 (2020).
- [52] T. Kinjo, S. Kajino, T. Nishio, K. Kawashima, Y. Yanagi, I. Hase, T. Yanagisawa, S. Ishida, H. Kito, N. Takeshita, K. Oka, H. Eisaki, Y. Yoshida, and A. Iyo, *Supercond. Sci. Technol.* **29**, 03LT02 (2016).
- [53] H. M. Tutuncu, E. Karaca, H. Y. Uzunok, and G. P. Srivastava, *Phys. Rev. B* **97**, 174512 (2018).
- [54] S. Sun, K. Liu, and H. Lei, *J. Phys.: Condens. Matter* **28**, 085701 (2016).
- [55] J. Chen, *J. Supercond. Novel Magn.* **31**, 1301 (2018).
- [56] M. Kakihana, H. Akamine, T. Yara, A. Teruya, A. Nakamura, T. Takeuchi, M. Hedo, T. Nakama, Y. Onuki, and H. Harima, *J. Phys. Soc. Jpn.* **84**, 124702 (2015).
- [57] D. Shao, X. Luo, W. Lu, L. Hu, X. Zhu, W. Song, X. Zhu, and Y. Sun, *Sci. Rep.* **6**, 21484 (2016).